The 11 March 2011 East Japan Earthquake and Tsunami:

Tsunami Effects on Coastal Infrastructure and Buildings

Harry Yeh

School of Civil & Construction Engineering, Oregon State University

Corvallis, Oregon 97331-3212, USA

harry@engr.orst.edu

Shinji Sato and Yoshimitsu Tajima

Department of Civil Engineering, the University of Tokyo

Hongo, Tokyo 113-8656, Japan

Abstract: The 11 March 2011 East Japan Earthquake and Tsunami caused unprecedented damage to well-engineered buildings and coastal structures. This report presents some notable field observations of structural damage based on our surveys conducted along the Sanriku coast in April and June 2011. Engineered reinforced concrete buildings failed by rotation due to the high-velocity and deep tsunami inundation: entrapped air in the buildings and soil liquefaction by ground shaking could have contributed to the failure. The spatial distribution pattern of destroyed and survived buildings indicates that the strength of tsunami was affected significantly by the locations of well-engineered sturdy buildings: weaker buildings in the shadow zone tended to survive while jet and wake formations behind the sturdy buildings enhanced the tsunami forces. We also found that buildings with breakaway walls or breakaway windows/doors remained standing even if the surrounding buildings were washed away or destroyed. Several failure patterns of coastal structures (seawalls) were observed. Flow-induced suction pressure near the seawall crown could have caused the failure of concrete panels that covered the infill. Remarkable destruction of upright solid-concrete type seawalls was closely related with the tsunami induced scour and soil instability. The rapid decrease in inundation depth during the return-flow phase caused soil fluidization down to a substantial depth. This mechanism explains severely undermined roads and foundations observed in the area of low flow velocities.

Keywords: tsunami, fluidization, breakaway wall, seawall, scour

Introduction

Prior to the 11 March 2011 East Japan Earthquake and Tsunami, the Sanriku Coast of northeastern Japan had been attacked by several giant tsunamis: most recently the 1896 Meiji Sanriku Tsunami, the 1933 Showa Sanriku Tsunami, and the 1960 Chilean Tsunami. The Chilean Tsunami was a distant-source tsunami that originated in Chile about 17,000 km away, and resulted in a maximum runup of 4.9 m at the Sanriku Coast (Takahashi and Hatori, 1961). Just like the 2011 Tsunami, the 1896 and 1933 Tsunamis were "local" or near-source tsunamis. Figure 1a compares tsunami runup distributions and the locations of those earthquake epicenters. The earthquake magnitudes for the 1896 and the 1933 Tsunamis were M 8.5 and Mw 8.4, respectively (USGS, 2010). The maximum runup height recorded in the 1896 tsunami was 38.2 m, whereas the 1933 tsunami generated runup heights up to 29.3 m (Iida, 1984). The 2011 Mw 9.0 earthquake event was much greater than the previous two, and the maximum reported tsunami runup height was nearly 40 m, which is comparable to the 1896 Meiji Tsunami. On the other hand, the tsunami-affected areas for the 2011 event were much larger. Both the 1896 and 1933 Tsunamis affected only the Sanriku coast (roughly spanning 38.25˚N to 40.5˚N), whereas the 2011 Tsunami affected (defined as runup heights of more than 5 m) more than 1000 km of the Japanese coastline ranging from the Chiba Prefecture (35.5˚N) in the south up to the Hokkaido Prefecture (43.0˚N) in the north. As shown in Fig. 1a, the runup pattern of the 2011 Tsunami is skewed to the south and its centroid is shifted far north from the earthquake epicenter, while the records of the previous Meiji and Showa Tsunamis exhibit bi-modal distributions (runup peaks at the two locations: 39˚N and at 40˚N). The 2011 Tsunami appears to present different characteristics from the 1896 and the 1933 events in terms of both the runup distribution pattern and the expanse of the affected area.

Wave profiles of the 2011 Tsunami were recorded at several locations along Japan's continental shelf with GPS buoys (PARI, 2011) as well as seafloor pressure transducers (ERI, 2011). Figure 1b shows compiled data of tsunami waveforms along the west-to-east transect line from the town of Kamaishi. Two of line-plots are data captured with seafloor pressure transducers (ERI, 2011) located at 45 km offshore in water depth of 1013 m, and at 73 km offshore in 1618 m of water. The other is measured by the GSP buoy (PARI, 2011) located at 15 km offshore in 204 m of water. The compiled plots demonstrate the tsunami evolution during its approach toward the shore. The temporal waveform closest to the shore (the GPS buoy) shows that the leading wave was a small negative wave with about 0.4 m wave height, followed by a gradual increase in water surface elevation, and then a rapid rise to reach a 6.7 m wave height. According to Synolakis (1991), tsunami's shoaling amplification can be estimated with Green's law: Green's law says that wave height is proportional to -¼ power to the water depth (e.g. Lighthill, 1978). Based on the measured wave amplitude of 6.7 m in water depth of 204 m, Green's law predicts a tsunami height of 14 m in a depth of 10 m, which is very large but comparable to the values obtained from field surveys – average tsunami height in the outer coast of Kamaishi is 15.7 m (extracted from The 2011 Tohoku Earthquake Tsunami Joint Survey Group, 2011). (Note that tsunami wave height predicted by Green's law at the water depth of 10 m is often used as a representative tsunami height at the shore: e.g. Takahashi (2011). From hereinafter, all of the runup heights presented in the paper are obtained from the 2011 Tohoku Earthquake Tsunami Joint Survey Group (2011) unless otherwise stated, and for brevity, this reference will be called Joint Survey Group.) The 2011 Tsunami was evidently very large and the presence of the sharp peak in the waveform must have played a primary role in creating high-velocity flows and transient inundation processes (Yeh et al., 2011).

This paper reports our observations and analyses on coastal structures and buildings based on the field surveys conducted April 12 – 13, and June 18 – 21, 2011. All of our field data are geo-referenced with the RTK GPS (Real-Time-Kinematic GPS System), elevations and distances were measured with laser rangefinders, and damages were recorded with GPS cameras.

Having learned the lessons from previous disasters, coastal structures in the Sanriku Area were well designed and constructed to withstand seismic and tsunami events. Yet, the 11 March 2011 East Japan Earthquake and Tsunami resulted in unanticipated consequences causing widespread and heavy damage. The 2011 Tsunami exceeded the capacity of coastal protection structures that were designed based on the 1896 Meiji, the 1933 Showa, and the 1960 Chilean Tsunamis. Prior to this event, well-engineered reinforced concrete (RC) structures were thought invulnerable to tsunamis. We prove that it is a myth. Tsunami's hydrodynamic forces, enhanced buoyant forces with entrapped air, and soil foundation instability by the preceding ground shaking could have contributed to the toppling of the RC buildings. On the contrary, we found some buildings that survived because of their breakaway walls and windows. A majority of the coastal protection structures (e.g. seawalls) failed due to soil instability triggered by earthquake shaking as well as tsunami actions.

Tsunami Damage: Buildings

The remarkable failure of reinforced concrete (RC) buildings was observed in the town of Onagawa. The average runup height in Onagawa was 17.9 m (Max. 20.4 m and Min. 15.8 m). Several RC buildings were overturned by tsunami waves, while the structures themselves were not broken up by wave impact (see Fig. 2). This rotation failure had not been reported in the past.

In fact, past tsunami surveys indicated that engineered RC buildings had been considered strong against tsunamis (Shuto, 1994).

Based on inundation data, the overturned buildings were fully (or at least nearly) submerged. We hypothesize that the buildings overturned by the following possible causes: a) hydrodynamic force including debris effects, b) buoyant force, and c) weakened foundation associated with soil instability. Note that hydrodynamic force is the lateral force induced by the flow and the buoyancy force is enhanced by trapped air. An additional cause could be debris-impact force on the buildings. According to video footage (Video, 2011), no large and rigid floating body (e.g. a ship) was present in the inundation flow, and a majority of debris was made of soft materials such as broken wood-frame houses and small automobiles.

Let us examine the failed four-story building shown in Fig. 2d. Considering its initial location – identified from the Google Map/Street View, the building was toppled, tumbled, and transported for more than 30 m inland; the failure must have occurred during the runup process. The steep hill embankment along the north side of the building (the left-hand side of the blue circle shown in Fig. 3b) could have acted as a flow guide causing flow contraction, and consequently enhanced the power. The building had a pile foundation but all of the piles were snapped at the building base. The building dimensions are approximately 16 m tall, 7 m wide and 7.5 m long, made with 130 m^3 of concrete (density = 2400 kg/m^3). The effective net weight of the building under total submergence is approximately 1800 kN. Without any flow, this weight would require about 180 m^3 of entrapped air to float the building, which is about a 1 m thick layer of entrapped air per story (four stories). Therefore, the failure caused solely by buoyant forces is possible even with no water flow, when the building is totally submerged and the pile foundation is ineffective.

Hydrodynamic force induced by tsunami flow can be estimated using the formula similar to that of the drag force (e.g. Yeh, 2007):

$$F = \tfrac{1}{2} C_D \rho A u^2 , \quad (1)$$

where $C_D \approx 2$ for a square-shaped building, ρ is the water density, A is the building frontal area perpendicular to the flow direction, and u is the flow speed. Under the condition with no entrapped air in the building and the flow impinging against the broader side (7.5 m) of the building, moment balance at the ground level yields the flow speed $u > 2.6$ m/sec required to topple the building. This flow speed is much slower than the flow speeds inferred from the video footage by Koshimura (2011): a maximum of 6.3 m/sec during the tsunami runup and 7.5 m/sec during the return flow. A runup flow speed of 6.3 m/sec exerts more than five times the required moment necessary to topple the building. It is emphasized that the required flow speed for failure would be reduced substantially if the buoyant effect by entrapped air were included. Additionally, debris accumulation against the building effectively increases the value of A in (1). Furthermore, any debris impact could have been an additional factor for the building failure. Note that debris impact was reported as a major cause for building damage in the previous tsunami events (e.g. the 2004 Indian Ocean Tsunami by Ghobarah et al., (2006) and Yeh, (2009); the 2009 Samoa Tsunami by Reese et al., (2011)). Our analysis demonstrates that the building can overturn even without the effect of debris impact. There is an added factor to further promote the overturning failure: that is the possibility of soil liquefaction due to strong ground shaking of the earthquake that had occurred about 40 minutes prior to the tsunami arrival. With soil liquefaction, the friction between the piles and the surrounding soils would be reduced. Even though this building had a pile foundation, the fast flow speeds and the deep inundation could have snapped the piles.

Based on the foregoing analysis, the combination of hydrodynamic force, entrapped air in the building, and soil liquefaction can provide an explanation for overturning failure of the building. The deep inundation flow that caused the buildings to be fully submerged and the high velocities resulting from the fast rise and fall of the tsunami (as shown in Fig. 1b) are two factors that caused the building failure by rotation. The similar analysis can be made for the other buildings failed by rotation (e.g. those shown in Fig. 2b and c). It is readily pointed out that for a given building weight (or volume), the hydrodynamic moment (torque) is smaller for a shorter building. Building failure by rotation depends on the dimensions, orientation, foundation, and air-tightness characteristic of the building.

In spite of such extraordinary failure of several RC buildings in Onagawa, two large RC buildings at the waterfront and the smaller buildings directly behind them were found standing (Fig. 3a). The damage pattern shown in the figure suggests that the waterfront buildings must have acted as a barrier for the smaller buildings behind them. Video footage (Video, 2011) shows a strong jet formation in the gap between the two large forward buildings, which wiped out everything in its path. Clearly, the presence of the sturdy RC buildings altered the tsunami flows, which in turn affected the surroundings. This type of observation is not new, however. Abe et al. (1993) reported reduction and enhancement of tsunami effects on the surroundings of sturdy buildings in the town of El Transito affected by the 1992 Nicaragua Tsunami. This indicates that tsunami resilient structures should be designed with consideration of the effects from the surroundings, which resembles the design practices for high-rise buildings and long-span bridges for wind forces. Recently Reese et al. (2011) incorporated the shielding effects in their building fragility analysis for the 2009 Samoa Tsunami.

We found that some of the structurally survived buildings were those in which ground-level walls were blown off by tsunami forces; in other words, the walls acted as so-called breakaway walls. Note that the similar observations have been made from the previous tsunami events: e.g. the 1992 Nicaragua Tsunami (Yeh, 1995) and the 2004 Indian Ocean Tsunami (Dalrymple and Kriebel, 2005). Figure 3c shows a typical example in Onagawa: the right panel of the figure shows the condition prior to the tsunami attack that we obtained from Google Maps/Street View. This building formed openings piercing from the front to the back aligned with the tsunami flow direction. Those openings were not designed for tsunami protection, but the tsunami forces punched through the windows and doors.

The apartment buildings in Rikuzen-Takata shown in Fig. 4 are another example. The average runup height in the vicinity of the buildings was 14.2m (Max. 15.3 m, and Min. 13.1 m). The inundation found in the apartment building was at 12.2 m reaching the top (5^{th}) floor. The fast jet formations through the pierced windows (Fig. 4b) enhanced the net momentum flux in the flow direction in comparison with the condition of a solid object, consequently reducing the tsunami force on the building. Note the complete destruction surrounding the surviving buildings (Fig. 4). The shielding effect discussed in Fig. 3 is also evident in the second apartment building. We see clear damage contrast in the front apartment unit facing the sea and the second unit behind it.

Scour and Foundation Failures

The most notable damage of coastal protection structures is attributed to scour and foundation failure. Figure 5b shows the seawall failure in Kanahama, near Miyako, where the average runup height was 11.3 m (Max. 12.6 m, Min. 10.6 m). The crown elevation of the seawall is 8.5 m TP so that the tsunami overtopped the seawall. (TP: Tokyo Pell is the Japanese sea-surface datum,

whereas tsunami runup heights are from the sea level at the time of tsunami attack. Note that the sea level at the time of the 2011 Tsunami was approximately 40 cm higher than TP.)

As shown in Fig. 5b, the front face of the seawall is intact with little damage. The rear face is severely undermined. Note that the sloping faces of the soil-mound infill are covered and protected by the concrete panels: note that the concrete slabs on the rear face is 25 cm thick. One section of the seawall is completely breached and a large scour-hole pond was formed behind the seawall. We found that the upper rear portion was damaged more than the lower portion as seen in Fig. 5b (in the far view). A possible explanation for this damage pattern is the suction pressure induced by the overtopping flow. Once the tsunami overtopped the seawall, the flow became quasi-steady and supercritical on the rear face. The centrifugal force associated with this downpour flow pattern induced suction-pressure force near the top portion of the rear side. Let us consider the critical flow condition at the crown with the specific energy of 3 m. Following the flow analysis of spillways by Henderson (1966), we assume the streamlines in the concentric circular formation. This circular streamline formation is closely related to the length scale of the flow-separation bubble formed on the rear 1:2 sloping surface. Assuming the radius of the inner streamline is 1.5 m, the suction pressure can be calculated to be 8.6 kPa (or 0.88 m of suction water head). This suction pressure force can lift a concrete slab of 37 cm thick even if the pressure underneath is atmospheric. Therefore, the centrifugal pressure is capable of lifting the concrete slab (25 cm thick) of the Kanahama seawall. It is anticipated that the pressure underneath the slab could be greater than the atmospheric pressure, because of the high tsunami inundation in front of the seawall and its infill that may not be completely impermeable. This could have induced positive pressure under the concrete slab creating the additional force for the panel failure. Once the protective concrete panels were removed, soil-infill was exposed to the

flow so that further scour failure in the seawall mound resulted. In addition, turbulent and high-velocity flow impingement on the rear toe of the seawall can create a large scour hole behind the seawall. We observed many seawalls that exhibit the similar failure pattern.

Figure 5c shows the failed seawall in the town of Kirikiri, where the average runup height was 17.1 m (Max. 19.0 m, Min. 13.9 m): the crown elevation of the seawall is 6.3 m TP so that the tsunami substantially overtopped the wall. This is an upright solid-concrete type seawall with a pile foundation. Deep scour was observed under both front and rear faces of the seawall. During the tsunami return flow, several seawall components were pushed out seaward and scattered on the beach. The failure mode observed suggests that the seawall was rotated counterclockwise forward (in the orientation shown in Fig. 5c) from the foot onto the adjacent beach. The seawall sections themselves were undamaged structurally; hence, this failure must be caused by soil instability in the foundation. The failure mode of the seawall segments indicates that the seaward foundation must have failed by the overtopping return flow, allowing the return-flow water to undermine the toe of seawall and push out the foot seaward.

The seawall condition in Hakozaki is shown in Fig. 5d: the average runup height in this town was 15.4 m (Max. 17.0 m, Min. 13.4 m). The seawall is also an upright solid-concrete type. Interestingly, this seawall was not damaged although the town was completed destroyed by the overtopped tsunami (the crown elevation is 5.6 m TP). There are reinforced concrete flanges (2 m wide) protecting both the front and rear toes of the seawall. In addition the drainage gutter along the rear flange (see Fig. 5d) could have helped prevent the rear wall from excessive scour.

The water pond between the two waterfront buildings shown in Fig. 3a is a very deep scoured hole (more than 3.5 m deep), where a road was located prior to tsunami inundation. Judging from the video footage (VIDEO, 2011), high-velocity and debris-laden return flow between the sturdy

RC buildings must be responsible for the formation of this deep scour hole. Figure 4c shows a scour hole observed at the side of the apartment building. Those tsunami effects on soils are typical and had been reported from previous tsunami field surveys, in particular the 2004 Indian Ocean tsunami (e.g. Dalrymple and Kriebel, 2005; Yeh et al., 2007). The following are additional observations of scour, but unlike the foregoing cases, we found deep scour in protected areas where flow velocity is low.

Figure 6 shows the damaged area on the seaward side of the seawall in the town of Tohni. The seawall is seen in the background of Fig. 6d, and its crown elevation is at 11.8 m TP. Tsunami overtopped the seawall: the average tsunami height was 15.5 m (Max. 17.4m; Min. 11.8 m). In spite of the significant inundation depth, we found two buildings still standing in front of the seawall. One of them is a 2-story steel-frame building, and the other is a small wood-frame shack (Fig. 6b). The tsunami flow power must have been weak enough for those buildings to survive. Nonetheless, we observed severe undermining damage in the road and scour under the building foundation (Fig. 6c and d). Considering the survived buildings, it is unlikely that shear forces or hydrodynamic lift forces that require high-velocity flows caused the substantial scour damage.

Tsunamis can rip out pieces of asphalt pavement. This phenomenon was found in roads, harbor quay surfaces, and parking lots at many low-elevation locations near the shore. In particular, the damage shown in Fig. 4d was found in the well-sheltered area behind the front apartment unit in Rikuzen-Takata. The destroyed pavement pieces accumulated behind the first apartment unit facing the ocean, suggesting that the failure occurred during the return flow phase. It is unlikely that this damage was cause by fast flow velocities. As we discuss in the next section, the damage could result in the uplift force induced by the pore-pressure gradients that developed during the process of rapid reduction of the flow depth.

Tsunami Induced Soil Instability

As discussed in Figs. 4 and 6, soil instability that triggers severe scour and undermining effects is not always associated with fast and violent tsunami flows. Consider the following hypothesis. During tsunami inundation, the soil surface is pushed downward by the water weight. This downward force causes the upper layers of soil to compress, and results in an increase in both pore pressure and total normal stress in the soil medium. Near the end of tsunami's return flow, the water level and water velocity subside. The pressure on the soil surface rapidly decreases and the slow rate of the pore-pressure dissipation creates a vertical gradient of 'excess' pore pressure within the soil (the 'excess' pressure is the pressure deviation from its gravity force balance or equivalently from the hydrostatic pressure). When the excess pore pressure gradient reaches the buoyant specific weight of the bulk saturated soil, the soil would be supported by the pore pressure alone. This state implies the loss of resistance to shearing forces; the soil behaves like a fluid. Such fluidization was demonstrated experimentally in a large wave flume by examining tsunami-induced scour around a vertical cylinder (Kato *et al.* 2000; Yeh *et al.* 2001).

The fluidization condition can be expressed as

$$-\frac{\partial p_e}{\partial z} \geq (\rho_b - \rho) g = \gamma_b \,. \tag{2}$$

Here, the coordinate z is directed vertically upward (the direction is the opposite of gravity), p_e is the excess pore water pressure or $p_e = p - \rho g (h - z)$ where h is the water depth above the soil bed, ρ_b is the bulk density of the saturated soil, ρ is the water density, and γ_b represents the buoyant specific weight of the saturated soil. If the tsunami inundation depth decreases rapidly, it

could cause the excess pore-pressure gradient to exceed the buoyant weight of the bulk soil. Even if the flow velocities over the soil were small, the top layer of soil could eject upward.

To analyze tsunami-induced fluidization, Tonkin *et al.* (2003) used the one-dimensional consolidation model proposed by Terzaghi (1925). Within this model, the excess pore-pressure, p_e, is expressed by the parabolic equation:

$$\frac{\partial p_e}{\partial t} = c_v \frac{\partial^2 p_e}{\partial z^2}, \tag{3}$$

where c_v is the coefficient of consolidation. The exact solution to (3) for infinite soil thickness, assuming that the surface pressure decreases linearly by the amount Δp_e over time ΔT, can be derived analytically (Carslaw and Jaeger, 1959). Combining the fluidization condition given by (2) yields the prediction for the depth d_s of the tsunami-induced fluidization:

$$d_s = \frac{\Delta p}{\gamma_b}\left(1 - 4\mathrm{i}^2\mathrm{erfc}\left[\frac{d_s}{2\sqrt{c_v \Delta T}}\right]\right), \tag{4}$$

where $\mathrm{i}^2\mathrm{erfc}[\bullet]$ is the second integral of the complementary error function.

Applying (4) to the tsunami runup-and-return-flow data measured in the town of Kesen-numa (Fritz et al. 2011), a layer thickness of fluidized soil d_s is calculated and the results are presented in Fig. 7. Note that Fritz et al. (2011) extracted the temporal variations of flow velocities and water-surface elevations from the video footage with the aid of ground based Lidar measurements. Here we used $\Delta p/\rho g$ = 8.5 m and ΔT = 10 minutes taken from the inundation history shown in Fig. 7, and the buoyant specific weight of the soil γ_b = 880 dynes/cm^3. Creating the condition to test for (3) and monitoring the pore pressures in the laboratory, Yeh et al. (2004) obtained the average value of consolidation coefficient c_v = 750 cm^2/sec with a range from 400

to 1200 cm^2/sec for Ottawa Fine Sand with D_{50} = 0.26 mm. Such a wide range of the variations is attributed mainly to a variety of soil compaction used in the experiments. The uncertainty in the value of the consolidation coefficient c_v as well as its high sensitivity to the fluidization depth d_s – see Fig. 7 – does not allow us to make an accurate estimate for the fluidized soil layer. Nonetheless, the result in Fig. 7 demonstrates that the rapid return flow of the 2011 Tsunami is capable of fluidizing the sandy soil down to a substantial depth. For example, the fluidized layer thickness is d_s = 290 cm for c_v = 750 cm^2/sec, d_s = 410 cm deep for c_v = 600 cm^2/sec, and d_s = 520 cm for c_v = 450 cm^2/sec. The maximum possible liquefaction depth is $d_s \to \Delta p / \gamma_b$ = 720 cm > 7 m! Therefore, the results suggest that the substantial development of excess pore-pressure gradients can trigger upward forces from underneath, which could have caused the scenes of ripped-out asphalt slabs shown in Fig. 4, as well as the severe scour hole and the undermined road (Fig. 6) in the town of Tohni: recall that flow velocities in those areas could not have been large judging from the surrounding damage conditions.

The traditional scour mechanism for steady flow is the bed shear stresses, but the excess pore-pressures play little role in the soil instability. On the other hand, tsunami flows are transient with the timescale of tens of minutes. The result shown in Fig. 7 demonstrates that the effects of pore-pressures can be substantial for the 2011 Tsunami. It is likely that the excess pore-pressure gradients contributed the damages such as the scour holes between the buildings shown in Fig. 3a and Fig. 4c, as well as the seawall failure in Kirikiri (Fig. 5c).

It must be cautioned however that the foregoing analysis involves some limitations. First, Terzaghi' consolidation model (3) is a linear model for the one-dimensional field. In realty, scour formations are three-dimensional, and the process is nonlinear because the consolidation coefficient c_v depends on the pore pressure. Second, the model assumes the condition of fully

pressurized and saturated soils at the time of maximum inundation; such condition occurred unlikely in the 2011 event because the runup process was not slow as shown in Fig. 7. In other words, the soils must have been less pressurized than the assumption, which could overestimate the fluidized depth d_s.

Conclusions

Prior to the 2011 Tsunami, the failure mode of reinforced concrete (RC) buildings by moment had not been reported, partly because no tsunami with that intensity had attacked a well-developed community with the presence of many RC buildings. When the tsunami inundation is deep enough to submerge the buildings and the flow speed is sufficiently high, the moment failure of RC buildings is no longer a surprise. In addition, entrapped air within the building, debris impact, as well as soil instability of the foundation can further promote the moment failure. It is important to inspect this failure mode when we design critical RC coastal structures and buildings.

Buildings with breakaway walls and breakaway holes (windows and doors) helped the buildings survive from tsunamis. The breakaway openings of the survived buildings were aligned with the tsunami flow direction. The existence of sturdy buildings altered tsunami flows. The shadow zone created behind such buildings can protect other buildings. On the other hand, the jet and wake formations emanating from the buildings can enhance the tsunami forces that could destroy buildings in the flow paths. Those local effects of tsunami forces had been reported and discussed previously, but the explicit evidence we observed casts a challenge in designing coastal structures and buildings in tsunami prone areas. The engineering design should be

performed with consideration of detailed local tsunami-flow interactions with the surroundings; this resembles the analysis for high-rise buildings or long-span bridges for strong wind forces.

We reported three damage conditions of seawalls. Along the Sanriku coast in Japan, seawalls were designed to protect the coastal communities from tsunamis. We found that soil instability played a major role in the failures. For the mound-type seawall in Kanahama (Fig. 5b), the centrifugal pressure force induced by the overtopping flow is capable of removing the concrete panels covered the rear face of the seawall. Furthermore, the fast flow velocities with intense turbulence resulted in severe undermining damage in the rear face of the seawall, as well as formation of a large scour hole behind. The solid upright type seawall in Kirikiri (Fig. 5c) was destroyed during the tsunami's return-flow phase. Scouring and undermining actions are the primary cause of the failure. The similar upright type in Hakozaki (Fig. 5d) was found to be almost undamaged. Unlike the one in Kirikiri, the seawall toes in both front and rear sides are protected with 2-m wide concrete flanges. These concrete flanges must have prevented the toes (especially the rear side) from being undermined. Regardless of the type of seawall, protection of the rear-side surface and the toe appears to be critical for avoiding failure when and if tsunamis overtop a seawall.

The rapid decrease in inundation depth observed for the 2011 Tsunami could have developed significant pore-pressure gradients in soils, and the resulting upward forces could cause surface pavements to be pushed out even in the low-flow-velocity shadow zone. This mechanism also explains why substantially undermined roads and foundations occurred in the area of Tohni where flow velocities could not be high. Tsunami-induced soil instability was significant for the 2011 Tsunami, because of its tsunami waveform with a rapid increase and decrease in water elevation (Fig. 1).

The 11 March 2011 East Japan Earthquake and Tsunami caused substantial damage in the reinforced-concrete buildings that we previously understood to be invulnerable and coastal protection structures that were designed specifically for tsunamis. Observations and preliminary analyses presented in this paper may provide some hints to promote further research.

Acknowledgments

This work was supported by the US National Science Foundation RAPID Program (1135768), the Oregon State University Edwards Endowment, and the Japan Science and Technology Foundation J-RAPID Program.

References

Abe, Kuniaki., Abe, Katsuyuki, Tsuji, Y., Imamura, F., Katao, H., Iio, Y., Satake, K., Bourgeois, J., Noguera, E., and Estrada, F. (1993) Fields survey of the Nicaragua Earthquake and Tsunami of September 2, 1992. Bill. Earthq. Res. Inst., Univ. Tokyo, vol. 68, 23 – 70.

Carslaw, H.S. and Jaeger, J.C., (1959). Conduction of Heat in Solids. Oxford University Press, Oxford, 510 pp.

Dalrymple, R.A., and Kriebel, D.L. (2005), Lessons in engineering from the tsunami in Thailand. The Bridge, 35, 4-13.

ERI: Earthquake Research Institute, the University of Tokyo: http://outreach.eri.u-tokyo.ac.jp/eqvolc/201103_tohoku/eng/

Fritz, H.M., Phillips, D.A., Okayasu, A., Shimozono, T., Liu, H., Mohammed, F., Skanavis, V., Synolakis, C.E., and Takahashi, T. (2012) The 2011 Japan tsunami current velocity measurements from survivor videos at Kesennuma Bay using LiDAR. Geophy. Res. Lett., 39, L00G23, doi:10.1029/2011GL050686

Ghobarah, A., Saatcioglu, M., and Nistor, I. (2006). The impact of the 26 December 2004 earthquake and tsunami on structure and infrastructure. Engineering Structures, 28 (2), 312-326.

Henderson, F.M. (1966). Open Channel Flow. Macmillan Co., New York, New York, 522 pp.

Iida, K. (1984), Catalog of tsunamis in Japan and its neighboring countries. Special Report, Aichi Institute of Technology, 52 pp.

Joint Survey Group: The 2011 Tohoku Earthquake Tsunami Joint Survey Group (2011). Nationwide field survey of the 2011 off the Pacific coast of Tohoku Earthquake Tsunami, J. Jap. Soc. Civil Eng., B. 67(1), 63-66.

Kato, F., Sato, S. and Yeh, H. (2000), Large-Scale Experiment on Dynamic Response of Sand Bed around a Cylinder due to Tsunami, Coastal Engineering 2000, ASCE, 1848-1859.

Koshimura, S. (2011), Field survey of the 2011 tsunami inundation in Tohoku District: towards comprehensive understanding of tsunami disaster. Pre-publication report presented in Takatsuki, Japan, July, 2011.

Lighthill, J. (1978). Waves in Fluids. Cambridge University Press, 504pp.

PARI: Port and Airport Research Institute, (2011). Urgent Survey of 2011 Great East Japan Earthquake and Tsunami Disaster in Ports and Coasts. *Technical Note No. 1231*. 200p.

Reese, S., Bradley, B.A., Bind, J., Smart, G., Power, W., and Sturman, J. (2011). Empirical building fragilities from observed damage in the 2009 South Pacific tsunami. Earth-Science Review, 107, 156-173.

Shuto, N. (1994). Building damage evaluation for the 1993 Okushiri tsunamis, Tsunami Engineering Technical Report No.11, DCRC, Tohoku University, 11-28 (in Japanese).

Synolakis, C.E. (1991). Green's law and the evolution of solitary waves, Phys. Fluids A 3(3), 490 – 492.

Takahashi, R. and Hatori, T. (1961). A summary report on the Chilean tsunami of May 1960. Report on the Chilean Tsunami, Field Investigation Committee for Chilean Tsunami. Dec. 1961.

Takahashi, T. (2011). Mechanism of Tsunami. Parity, 26 (11), 34-41 (in Japanese).

Terzaghi, K. (1925). Erdbaumechanik (in German). Franz Deutike, Vienna.

Tonkin, S., Yeh, H., Kato, F., and Sato S. (2003). Tsunami Scour around a Cylinder: an Effective Stress Approach, Journal of Fluid Mechanics, 496, 165-192.

USGS, (2010). http://earthquake.usgs.gov/earthquakes/world/events/

Video: http://www.youtube.com/watch?v=2lnMZIRbLjM; http://www.youtube.com/watch?v=XbdCwe8agRQ&feature=related

Yeh, H. (1995). Tsunami Reconnaissance Procedures. Proceedings of the 27th Joint Meeting of US-Japan Panel on Wind and Seismic Effects, Tsukuba, Japan. 527-544.

Yeh, H. (2007), Design tsunami forces for onshore structures, J. Disaster Research, 2. 531-536.

Yeh (2009). Tsunami impact on coastlines. In: The Sea, Tsunamis (Ed: E.N. Bernard and A.R. Robinson), Harvard Univ. Press, 333-369.

Yeh, H., Kato, F., and Sato, S. (2001). Tsunami scour mechanisms around a cylinder. Tsunami Research at the End of a Critical Decade (Ed: G.T. Hebenstreit), Kluwer Academic Publishers. 33-46

Yeh, H., Tonkin, S., Heller, E., Arduino, P., Kato, F., and Sato, S. (2004). Mechanisms of scour induced by tsunami runup. Proceedings of Seccond International Conference on SCOUR and EROSION, Singapore. Vol. 2, 464-471.

Yeh, H., Francis, M., Peterson, C., Katada, T., Latha, G., Chadha, R.K., Singh, J.P., and Raghuraman, G. (2007). Effects of the 2004 Great Sumatra Tsunami: Southeast Indian Coast, Journal of Waterway, Port, Coastal, and Ocean Engineering, 133, 382-400.

Yeh, H., Sato, S. and Tajima, Y. (2011). Waveform evolution of the 2011 East Japan Tsunami. In: Asian and Pacific Coasts 2011: Proceedings of the 6th Intenational Conference on APAC 2011 (Ed: Lee, J. H.-W. and Ng, C.O.), World Scientific, Singapore. 131 – 138.

Figure Captions

Figure 1. (a) Survey data of tsunami runup height from the 11 March 2011 East Japan Earthquake and Tsunami. Also shown are the runup height distributions of the 1896 Meiji Tsunami and the 1933 Showa Tsunami (Japan Tsunami Trace Database: http://tsunami3.civil.tohoku.ac.jp/tsunami/mainframe.php). In the map, the locations of the earthquake epicenter that generated those tsunamis are shown. (b) Temporal tsunami waveforms η captured at the location (39˚14'56.0"N 142˚26'28.1"E) 15 km deep in a water depth of 204 m off Kamaishi (red line) and at (39˚13'52.3"N 142˚46'06.1"E) 45 km deep in 1013 m of water offshore (green line) and at (39˚15'31"N 142˚05'49"E) 73 km deep in 1618 m of water offshore (black line). Those data are extracted from PARI (2011) and ERI (2011). The location of Kamaishi City is marked as the red circle in (a).

Figure 2. Toppled reinforced concrete buildings in Onagawa (38˚26.5'N, 141˚26.5'E). The average runup height was 17.9 m. (a) The location of Onagawa. (b – d) Reinforced concrete buildings toppled by tsunami. (The photo (d) was taken by Koshimura).

Figure 3. Tsunami destruction pattern in Onagawa (38˚26.5'N 141˚26.5'E). (a) A pair of sturdy large buildings at the waterfront acted like barriers for some of the weaker buildings behind. (b) An areal view (the photo was enhanced from the original taken by Satake). The waterfront buildings can be identified in the photo. The gap between the buildings created a jet flow that completely destroyed the narrow strip of the jet trajectory, and caused a deep scour hole in-between. The blue circle shows the location of the toppled building shown in Fig. 2d, approximately 200 m from the waterfront. (c) The RC building severely damaged

but standing. The walls on the ground floor were punched away by tsunami. The right panel shows the conditions prior to the 2011 tsunami, taken from the GoogleMaps/StreetView.

Figure 4. The RC apartment buildings survived in Rikuzen-Takata. The average runup height in the vicinity was 14.2 m. (a) The location of Rikuzen-Takata (39˚00.5'N 141˚38.3'E). (b) The tsunami punched through from the front to back doors and windows to create many piercing holes, which must have reduced tsunami forces. (c) A deep scour hole at the side of the first building facing to the sea and (d) the ripped asphalt slabs in the sheltered area behind the first building.

Figure 5. Seawall failures. (a) From north to south, locations of Kanahama (39˚35.5'N 141˚56.8'E), Kirikiri (39˚22.3'N 141˚56.7'E), and Hakozaki (39˚19.4'N 141˚54.8'E). (b) Seawall failure in Kanahama with average runup height of 11.3 m. (c) Seawall failure in Kirikiri with average runup height of 17.1 m. (d) Seawall in Hakozaki was intact with little damage; average runup height was 15.4 m.

Figure 6. Undermined road and building foundations on the sea side of the seawall in Tohni. (a) The location of Tohni: the average runup height was 15.5m (39°12.5'N 141°53.2'E). (b) A couple of buildings survived from the tsunami inundation. (c) The size of the undermined road shown is 1.5m deep and 1.5 m high. (d) The size of the undermined foundation is 1.2 m high and 2.0 m deep.

Figure 7. (a) Time history of tsunami inundation depth in the town of Kesen-Numa, extracted from video footage (after Fritz et al., 2012). (b) Predicted liquefaction thickness vs. the consolidation coefficient c_v due to rapid reduction of the tsunami inundation depth as described in equation (4).

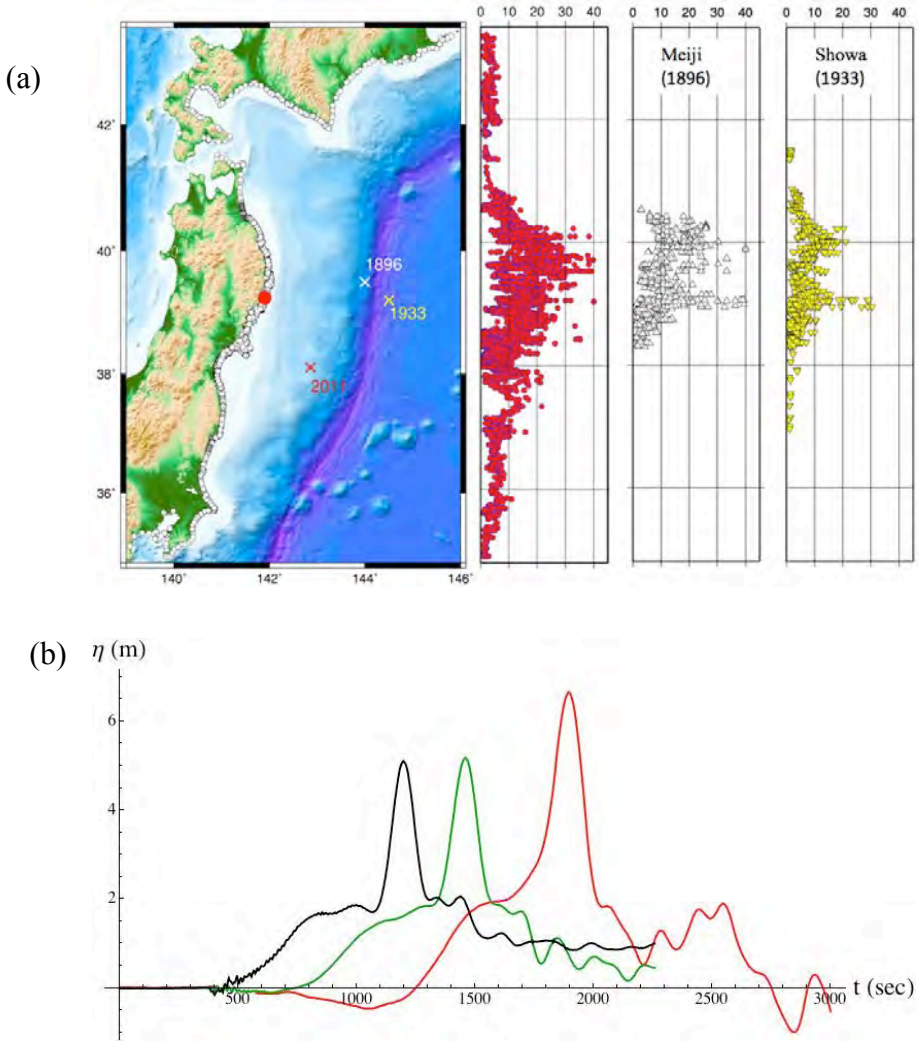

Figure 1. (a) Survey data of tsunami runup height from the 11 March 2011 East Japan Earthquake and Tsunami. Also shown are the runup height distributions of the 1896 Meiji Tsunami and the 1933 Showa Tsunami (Japan Tsunami Trace Database: http://tsunami3.civil.tohoku.ac.jp/tsunami/mainframe.php). In the map, the locations of the earthquake epicenter that generated those tsunamis are shown. (b) Temporal tsunami waveforms η captured at the location (39°14'56.0"N 142°26'28.1"E) 15 km deep in a water depth of 204 m off Kamaishi (red line) and at (39°13'52.3"N 142°46'06.1"E) 45 km deep in 1013 m of water offshore (green line) and at (39°15'31"N 142°05'49"E) 73 km deep in 1618 m of water offshore (black line). Those data are extracted from PARI (2011) and ERI (2011). The location of Kamaishi City is marked as the red circle in (a).

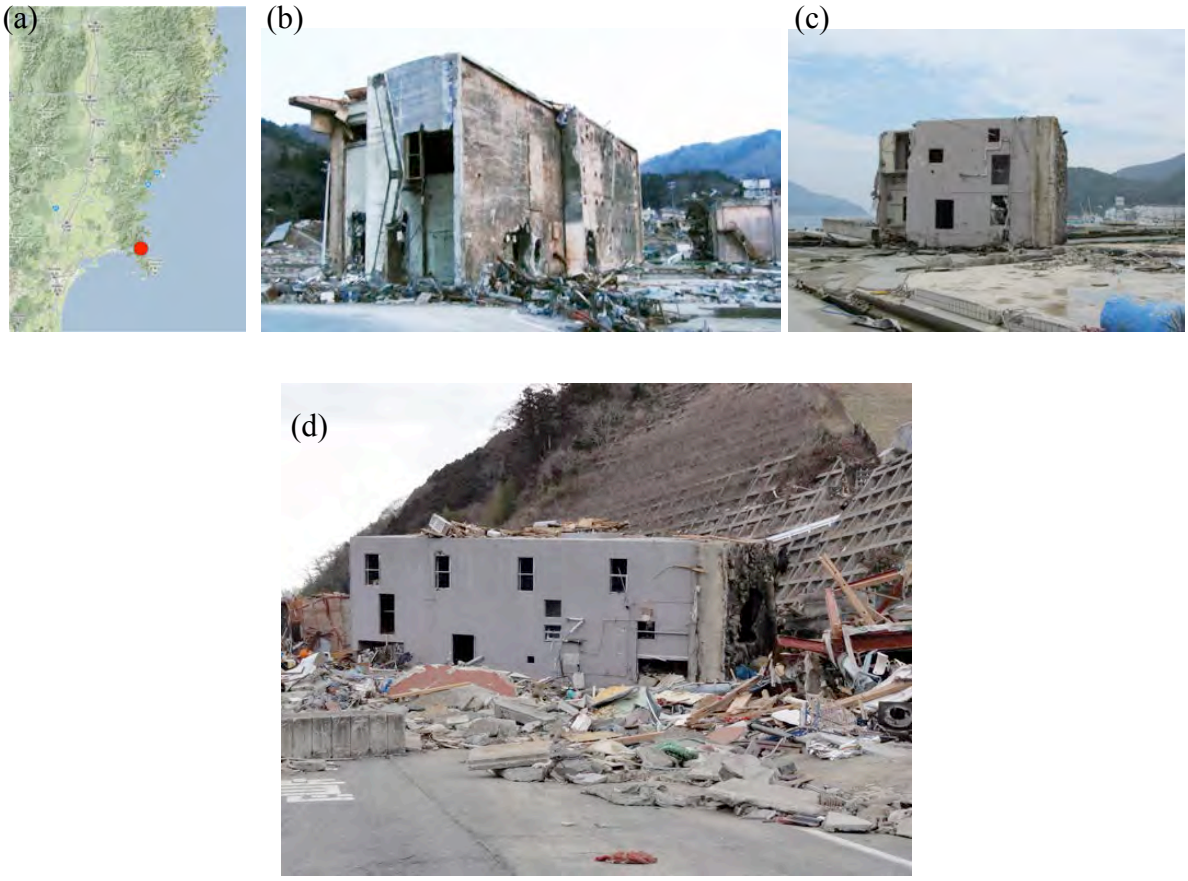

Figure 2. Toppled reinforced concrete buildings in Onagawa (38˚26.5'N, 141˚26.5'E). The average runup height was 17.9 m. (a) The location of Onagawa. (b – d) Reinforced concrete buildings toppled by tsunami. (The photo (d) was taken by Koshimura).

Figure 3. Tsunami destruction pattern in Onagawa (38˚26.5'N 141˚26.5'E). (a) A pair of sturdy large buildings at the waterfront acted like barriers for some of the weaker buildings behind. (b) An areal view (the photo was enhanced from the original taken by Satake). The waterfront buildings can be identified in the photo. The gap between the buildings created a jet flow that completely destroyed the narrow strip of the jet trajectory, and caused a deep scour hole in-between. The blue circle shows the location of the toppled building shown in Fig. 2d, approximately 200 m from the waterfront. (c) The RC building severely damaged but standing. The walls on the ground floor were punched away by tsunami. The right panel shows the conditions prior to the 2011 tsunami, taken from the GoogleMaps/StreetView.

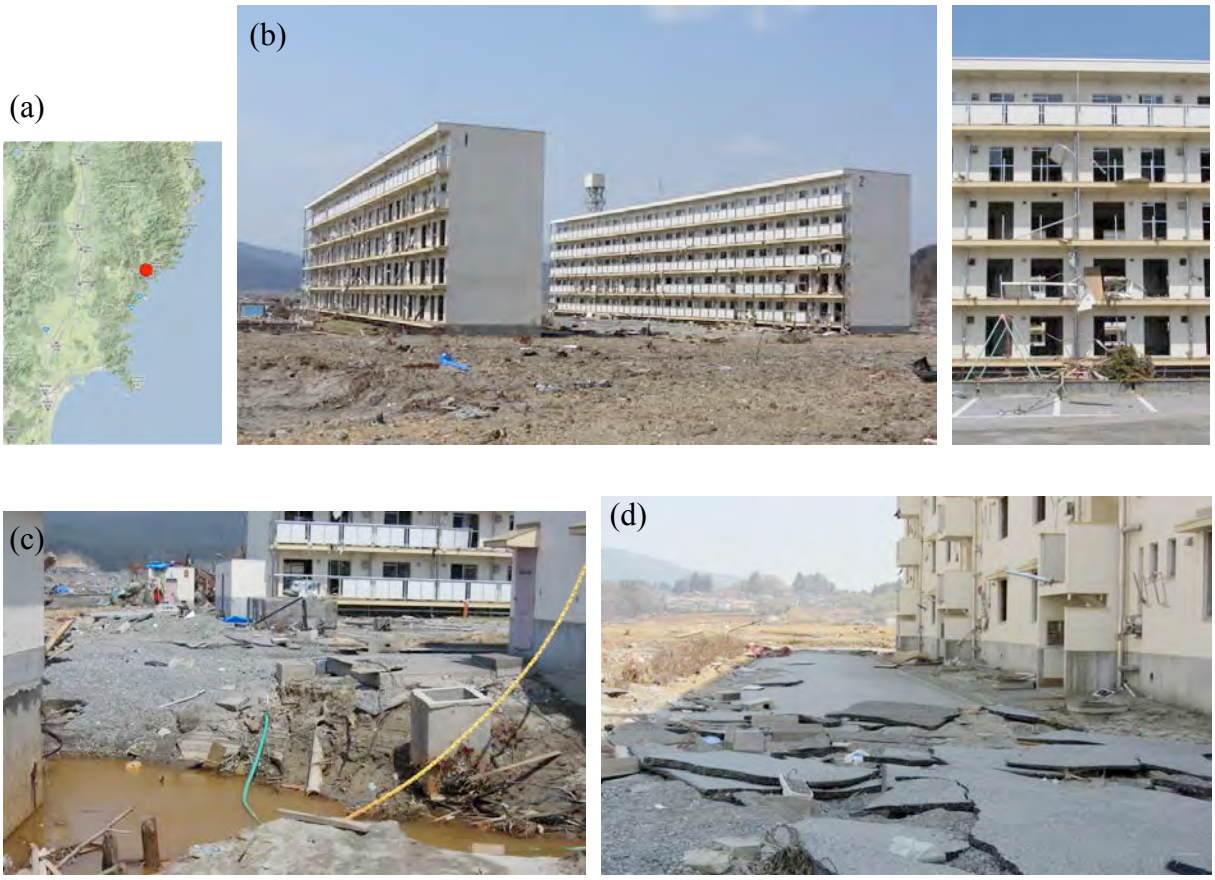

Figure 4. The RC apartment buildings survived in Rikuzen-Takata. The average runup height in the vicinity was 14.2 m. (a) The location of Rikuzen-Takata (39˚00.5'N 141˚38.3'E). (b) The tsunami punched through from the front to back doors and windows to create many piercing holes, which must have reduced tsunami forces. (c) A deep scour hole at the side of the first building facing to the sea and (d) the ripped asphalt slabs in the sheltered area behind the first building.

(d)

Figure 5. Seawall failures. (a) From north to south, locations of Kanahama (39˚35.5'N 141˚56.8'E), Kirikiri (39˚22.3'N 141˚56.7'E), and Hakozaki (39˚19.4'N 141˚54.8'E). (b) Seawall failure in Kanahama with average runup height of 11.3 m. (c) Seawall failure in Kirikiri with average runup height of 17.1 m. (d) Seawall in Hakozaki was intact with little damage; average runup height was 15.4 m.

Figure 6. Undermined road and building foundations on the sea side of the seawall in Tohni. (a) The location of Tohni: the average runup height was 15.5m (39°12.5'N 141°53.2'E). (b) A couple of buildings survived from the tsunami inundation. (c) The size of the undermined road shown is 1.5m deep and 1.5 m high. (d) The size of the undermined foundation is 1.2 m high and 2.0 m deep.

(b)

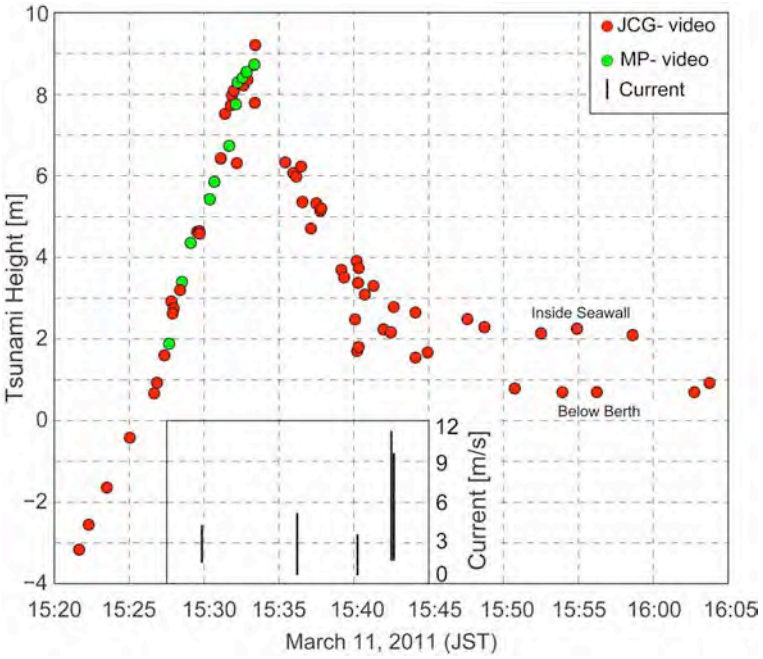

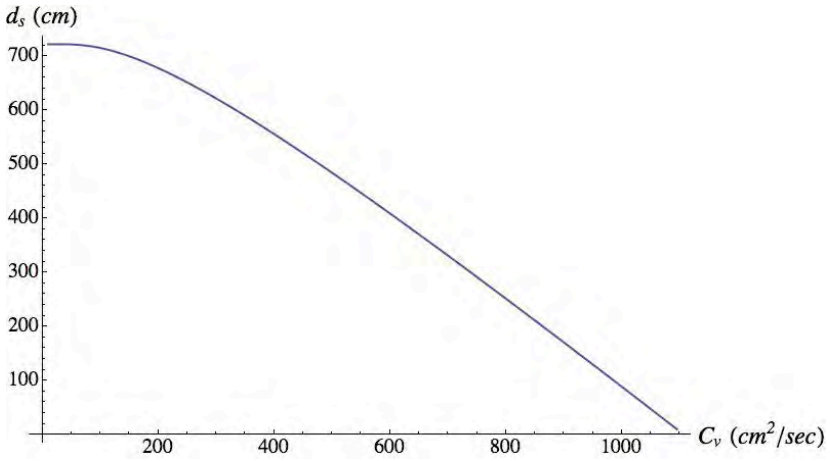

Figure 7. (a) Time history of tsunami inundation depth in the town of Kesen-Numa, extracted from video footage (after Fritz et al., 2012). (b) Predicted liquefaction thickness vs. the consolidation coefficient c_v due to rapid reduction of the tsunami inundation depth as described in equation (4).